FEBS Letters 588 (2014) 1949–1954

journal homepage: www.FEBSLetters.org

# The flanking sequence contributes to the immobilisation of spermine at the G-quadruplex in the NHE (nuclease hypersensitivity element) $III_1$ of the c-*Myc* promoter

Max A. Keniry *, Elisabeth A. Owen

*Research School of Chemistry, The Australian National University, Canberra, ACT 0200, Australia*

ARTICLE INFO

*Article history:*
Received 21 January 2014
Revised 28 March 2014
Accepted 2 April 2014
Available online 13 April 2014

Edited by Ivan Sadowski

*Keywords:*
DNA recognition
NMR spectroscopy
Spermine
Quadruplex DNA
c-Myc regulation

ABSTRACT

**Defining the molecular basis of the DNA sequence selectivity of polyamine binding is central to understanding polyamine-dependent gene expression. We have studied, by selective NMR experiments, the variation of spermine mobility and conformation in the presence of G-quadruplexes formed by sequences of the purine-rich strand of the c-*Myc* promoter, nuclease hypersensitivity element $III_1$ (NHE $III_1$). All the NHE quadruplexes restrict spermine mobility and induce a spermine conformational change but the most effective immobilisation occurs when all five G-tracts of the NHE $III_1$ are present. This suggests structure within the nucleotides flanking the G-quadruplex has a role in immobilising spermine.**



## 1. Introduction

There is an increasing body of evidence that polyamines influence specific gene expression especially oncogenes [1], but a detailed understanding of the molecular basis of this influence remains elusive. Rigorous control of cellular polyamine concentration is essential for the proper function of various cellular processes including gene transcription and translation, apoptosis [2] and chromatin remodelling [3]. Low polyamine concentrations are associated with the inhibition of cell growth [3], whereas up-regulation of polyamine synthesis is associated with pathological outcomes especially cancer [3,4]. Nevertheless, within this regime of strict regulatory control, polyamine concentration varies through the cell cycle.

The nuclease hypersensitivity element $III_1$ (NHE $III_1$) of c-*Myc* is a highly conserved 27-nt sequence upstream from the P1 promoter that controls 80–95% of c-*Myc* transcription [5]. There is evidence, that within the NHE $III_1$, one or more of the possible G-quadruplex isomers, which form under the influence of negative supercoiling, is a transcriptional repressor [6]. Conversely, a recent report indicated that polyamine-induced G-quadruplex formation is a transcriptional enhancer [7]. The wild-type G-rich strand of the NHE $III_1$ contains five tracts of three or more consecutive guanines, labelled I-II-III-IV-V (Pu27, Table 1). Several different G-quadruplexes are possible within the NHE $III_1$, but the major component, *in vitro*, is the parallel-stranded quadruplex (Fig. 1) formed from the four 3′-terminal G-tracts, II-III-IV-V with a 1:2:1 chain-reversal loop arrangement [8]. A minor component, the quadruplex formed from G-tracts I-II-IV-V with a 1:6:1 loop arrangement, is also present [9]. However, recent evidence suggests, that under the influence of negative superhelicity, the dominant G-quadruplex isomer is formed from the first four G-tracts, I-II-III-IV [10], even though, *in vitro*, this latter quadruplex has lower thermostability than the 1:2:1 quadruplex from G-tracts II-III-IV-V [11]. In the case of the 1:2:1 isomers, the structure of the unused G-tract in Pu27 is not definitively known but these flanking bases are likely to stack over an external G-quartet, causing the chain to fold back and form a pocket as shown diagrammatically in Fig. 1. In the 1:6:1 isomer, the third G-tract forms a long chain-reversal loop, which is probably more mobile than the short chain-reversal loops.

Because polyamines are small multivalent cations, they move in close association with slowly tumbling, highly charged anions

*Abbreviations:* bp, base-pair; CD, circular dichroism; NHE $III_1$, nuclease hypersensitivity element $III_1$; NMR, nuclear magnetic resonance; NOE, Nuclear Overhauser Effect; NOESY, Nuclear Overhauser Effect spectroscopy; nt, nucleotide; SCP, selective cross-polarisation; TBA, thrombin-binding aptamer; TOCSY, total correlation spectroscopy

* Corresponding author. Fax: +61 2 61250750.
*E-mail address:* max@rsc.anu.edu.au (M.A. Keniry).

http://dx.doi.org/10.1016/j.febslet.2014.04.003

**Table 1**
Oligonucleotides used in this study.

| Name | Sequence 5'-3' |
|---|---|
| | 1 2 3 4 5 6 7 8 9 10 11 12 13 14 15 16 17 18 19 20 21 22 23 24 25 26 27 |
| Pu27 | TGGGGAGGGTGGGGAGGGTGGGGAAGG |
| | I II III IV V |
| Myc12345 | TGGGGAGGGTGGGGAGGGTGGGGA |
| Myc1234 | TGGGGAGGGTGGGGAGGGT |
| Myc2345 | TGAGGGTGGGGAGGGTGGGGAA |
| | 1 2 3 4 5 6 7 8 9 10 11 12 13 14 15 16 17 18 19 |
| VEGFT | TGGGAGGGTTGGGGTGGGT |
| TBA | GGTTGGTGTGGTTGG |
| TGT | TGGGGT |

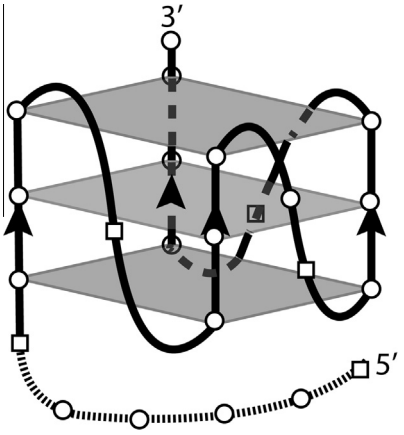


**Fig. 1.** Schematic representation of the major isomer of the parallel quadruplex with three chain-reversal loops formed by the NHE $III_1$ sequences and VEGFT. The dashed extension indicates the proposed location of the fifth G-tract of Myc12345. Guanines are indicated with circles and adenine and thymine by squares.

such as DNA. Nuclear magnetic resonance (NMR) diffusion studies confirm, that at low polyamine-DNA ratios, the polyamine diffusion closely mirrors the DNA diffusion [12]. NOE (Nuclear Overhauser Effect) NMR spectroscopy has provided valuable insights into the mobility, structure and affinity of DNA-bound polyamines. Positive $^1$H NOE peaks for spermine in the presence of B-DNA are consistent with substantial rotational and translational motions that are independent of the slow tumbling of the DNA, which is in accord with a loose association of spermine with the DNA [13] and the absence of polyamine electron density in X-ray studies [14]. Subsequent work with Z-DNA-forming oligonucleotides showed negative spermine NOE peaks consistent with a net slowing of the independent local motions of spermine [12,15]. The relative intensity of the intramolecular $^1$H NOEs also hinted at a possible divergence from the dominant all-*trans* conformation of free spermine and the potential for specific long-lived residence sites on Z-DNA. Negative NOEs are also observed for spermine associated with folded G-quadruplexes but not for a model four-stranded parallel G-quadruplex [16,17].

We have expanded on these earlier studies by employing $^{13}$C-labelled spermine and a series of selective $^1$H-detected, $^{13}$C-edited NMR experiments to more fully define the conformation of bound spermine in the presence of the thrombin-binding aptamer [18]. The selectivity of these experiments permits the quantitation of changes in the spermine NOE peaks by suppressing the DNA peaks. The evidence suggests that spermine adopts either a curved or a bent conformation that matches the curvature of the narrow grooves of the aptamer and makes contact with the loops that cap the grooves. At submillimolar concentrations of DNA and spermine, the two most sensitive of these NMR experiments provide complementary evidence for spermine conformational changes in the presence of G-quadruplexes. A comparison of the relative intensity of the intramolecular $^1$H NOEs generated on excitation of $\alpha2''$ protons (derived from the results of a 1D doubly-selective $^1$H/$^{13}$C cross-polarisation, NOE experiment, SCP($\alpha2''$)-NOESY [18]) is used to monitor the degree of spermine immobilisation and the tendency of spermine to adopt a curved or a bent conformation at the binding site [18]. A selective 1D($\alpha1$,$\alpha2'$)-zTOCSY experiment monitors the tendency of the central aminobutyl segment to adopt a *gauche* conformation about the C6–C7 and C6′–C7′ bonds by comparing the relative rate of magnetisation transfer along the $\alpha1$-$\beta$ and the $\alpha2'$-$\gamma$ TOCSY pathways [18].

A recent report that the interaction of polyamines with a DNA quadruplex formed at the NHE $III_1$ of the c-*Myc* promoter affects *c-Myc* gene expression [7] encouraged our investigation of the mobility and conformational tendencies of spermine in the presence of a number of oligonucleotides from the G-rich strand of the NHE $III_1$. The quadruplex-forming sequences of the NHE contain, G-tracts I-II-III-IV-V (Myc12345), I-II-III-IV (Myc1234) and II-III-IV-V (Myc2345). These data are compared with a closely related sequence from the VEGF promoter (−1805 to −1788 bp upstream of the transcription start site) [19] and two other G-quadruplexes that we have previously studied [16]. The former is labelled VEGFT to distinguish this sequence from the other quadruplex-forming VEGF sequence [20]. The NHE and VEGFT sequences are expected to form quadruplexes with a parallel-strand alignment and the NHE sequences have a 1:2:1 chain-reversal loop arrangement (1:2:1 describes the length of the three chain-reversal loops, Fig. 1). Thrombin-binding aptamer (TBA) is the thrombin-binding aptamer sequence [21] and TGT is a four-stranded parallel quadruplex [22] (Table 1). Herein, we show by selective NMR experiments that spermine changes shape and experiences a net reduction in mobility in the presence of the NHE $III_1$ G-quadruplexes but the greatest degree of immobilisation requires all five G-tracts within the NHE $III_1$.

## 2. Materials and methods

[$^{13}C_2$]-spermine was synthesised as described previously [16]. The oligonucleotides were synthesised and HPLC-purified by Geneworks (Adelaide, Australia) and dialysed in buffer extensively prior to use. Except for TBA and TGT, the quadruplex samples were dissolved in 250 µl Tris (10 mM), KCl (100 mM), 90% H2O/10% D2O, pH 7.0 buffer. The TBA sample was dissolved in phosphate (10 mM), KCl (100 mM), 90% H2O/10% D2O, pH 7.0 buffer. The TGT sample was dissolved in Tris (10 mM), NaCl (100 mM), 90% H2O/10% D2O, pH 7.0 buffer. The quadruplex concentrations were estimated by using UV spectrophotometry. The quadruplex samples were annealed by heating in buffer at 90 °C for 10 min then slowly cooled to room temperature followed by overnight equilibration at 4 °C. [$^{13}C_2$]-spermine was titrated into the quadruplex solutions from a concentrated spermine solution to a final spermine:quadruplex molar ratio of 1:1 for NMR and up to 20:1 for the circular dichroism experiments.

### 2.1. Circular dichroism (CD) spectroscopy

Circular dichroism spectra were recorded on an Applied Photophysics, Chirascan Circular Dichroism Spectrometer (Applied Photophysics Ltd., Leatherhead, UK) in a 10 mm path length quartz cell at 20 °C. The response time, the scanning speed and the wavelength range were respectively 0.5 s, 60 nm/min, and 220–320 nm. All CD spectra were zero-corrected and baseline-corrected for signal contributions due to buffer. The spermine was titrated into the quadruplex samples up to 20 mole equivalents.

### 2.2. Nuclear magnetic resonance (nmr) spectroscopy

All NMR spectra were recorded in 5 mm Shigemi NMR tubes (Shigemi Inc., Alison Park PA, USA) on a Varian INOVA-500 spectrometer (Agilent Technologies, Santa Clara CA, U.S.A) operating at a $^1$H frequency of 500.0 MHz and equipped with a z-axis indirect detection probe. Water suppression was accomplished by either z-dephasing gradients, presaturation or by non-excitation using the 11echo sequence [23]. All experiments were recorded at 15 °C unless specifically stated in the Figure legends. The doubly selective 1D-SCP-NOESY (200 ms mixing time) and 1D-zTOCSY (33 ms DIPSI-2 mixing period) experiments are described in detail elsewhere [18]. The doubly selective cross-polarisation (SCP) element employed simultaneous matched $^1$H/$^{13}$C spin-lock fields (170 Hz) applied for 4.7 ms at the $^1$H and $^{13}$C carrier frequencies 3.2 ppm and 46 ppm respectively. All other $^1$H selective excitation was achieved with the DPFGSE pulse scheme [24]. Typically the spectra were acquired with 16 k complex data points over a sweep width of 5000 Hz with a recycle time of 2 s except the 11echo pulse sequence, which had 32 k data points over a sweep width of 9000 Hz. All spectra were processed using either V NMR 3.2 or iNMR Reader 4.3 software (http://www.inmr.net) and apodised with 5–10 Hz exponential weighting functions. Peak areas were quantitated with the deconvolution routine in iNMR Reader.

### 2.3. Molecular modelling

The molecular models in Figs. 3, S3 and S4 were created using coordinates from the sequence, TGAGGGTGGGTAGGGTGGGTAA (PDB ID: 1XAV) [25] and visualised with the program, Chimera [26]. A curved spermine molecule [18] was manually placed over the 2-nt chain-reversal loop of 1XAV and the binding location optimised using the program, DOCK v6.5 [27]. A docking box of dimensions, 6.0 × 0.9 × 8.6 nm, with a grid spacing of 0.03 nm was created over the chain-reversal loop bounded by G12, G13, T14, A15 and G16. The G-quadruplex was fixed and the spermine was allowed to translate and rotate around the target. The most populated conformational cluster with the lowest binding energy was chosen. Electrostatic potential energy surfaces were calculated with the programs APBS [28] and MSMS [29] and visualised with Chimera [26].

## 3. Results and discussion

All the sequences from the NHE III$_1$ and VEGFT have circular dichroism (CD) profiles indicative of parallel quadruplexes. Spermine:DNA up to a 20:1 molar ratio has little effect on the spectra at 100 mM K$^+$ (Fig. S1). There is a minor loss of intensity of Myc1234

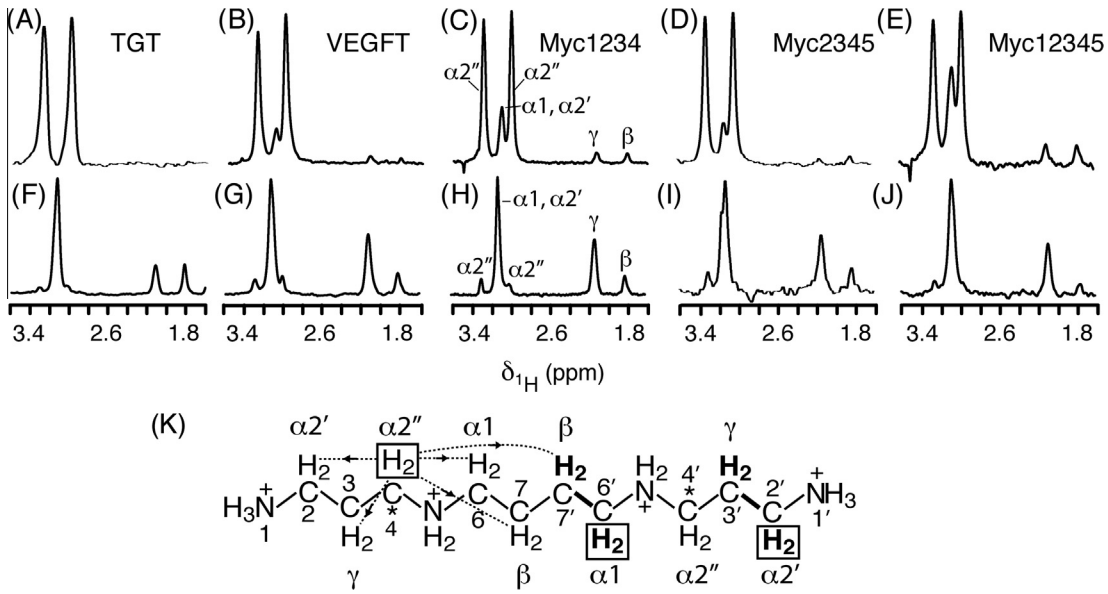


**Fig. 2.** (A–E) SCP(α2″)-NOESY spectra – (A) 1:1 $^{13}$C-spermine:TGT, (B) 1:1 $^{13}$C-spermine:VEGFT, (C) 1:1 $^{13}$C-spermine:Myc1234, (D) 1:1 $^{13}$C-spermine:Myc2345, (E) 1:1 $^{13}$C-spermine:Myc12345. (F–J) 1D(α1,α2′)-TOCSY spectra – (F) 1:1 $^{13}$C-spermine:TGT, (G) 1:1 $^{13}$C-spermine:VEGFT, (H) 1:1 $^{13}$C-spermine:Myc1234, (I) 1:1 $^{13}$C-spermine:Myc2345, (J) 1:1 $^{13}$C-spermine:Myc12345. (K) A labelled spermine structure. The asterisks indicate the $^{13}$C-labelled carbons and the boxed protons indicate the sites of selective excitation. Dotted lines (LHS) indicate the NOE pathways and bold lines and bold characters (RHS) indicate the TOCSY pathways.

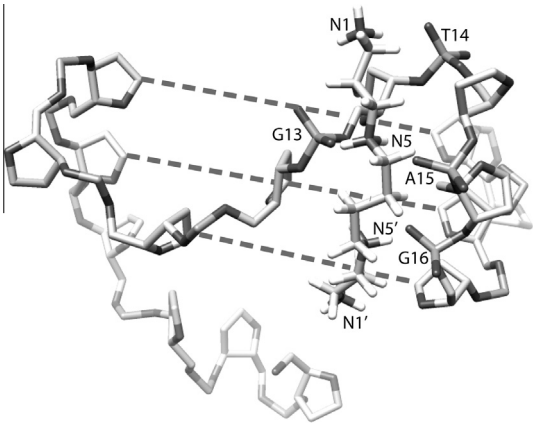


**Fig. 3.** Backbone representation of an analogue of the Myc2345 G-quadruplex (PDB entry: 1XAV) showing a possible location for a spermine binding site at the groove formed by the 2-nt chain-reversal loop and the second strand. Close contacts between spermine amino groups and quadruplex phosphates are labelled. The G-quartet positions are indicated with broken lines.

at 20:1 and this may be a reflection of the reported lower stability of this sequence [11]. We also observe only very minor changes in the $^1$H NMR spectra of the quadruplex imino proton resonances on titration with spermine (Fig. S2). This confirms earlier observations that spermine has little effect on the structure of DNA G-quadruplexes at meaningful cation concentrations [16].

The results of the SCP(α2″)-NOESY and the 1D(α1,α2′)-zTOCSY experiments are shown in Fig. 2A–E and Fig. 2F–J, respectively. All spectra are acquired under identical conditions. A diagram of spermine in the extended conformation with the protons labelled with Greek letters and the carbons labelled numerically is shown below the spectra in Fig. 2K. In the left half of the molecule, the NOE through-space pathways are indicated by broken lines and, in the right half of the molecule, the total correlation spectroscopy (TOCSY) through-bond pathways are shown in bold. The Nuclear Overhauser Effect spectroscopy (NOESY) mixing time of 200 ms ensures that the normalised NOEs are in the linear part of the NOE buildup curve [18] and the TOCSY mixing period of 33 ms measures the direct TOCSY transfer between *J*-coupled protons. In the SCP(α2″)-NOESY experiments, the α2″ proton resonance is selectively inverted and the normalised NOE intensities at the α1 + α2′, β and γ resonances are compared for each 1:1 $^{13}$C-spermine:quadruplex complex. The intensity of the NOEs is dependent on the apparent correlation time, the exchange between different chemical sites [30] and the $^1$H internuclear distances of spermine at each site. All the spermine NOEs in the TGT:spermine spectrum (Fig. 2A) are nulled indicating the apparent correlation time, which is a function of the slow tumbling rate of the TGT quadruplex and the faster independent motions of spermine, is ~0.3 ns. This is much shorter than the 3 ns rotational correlation time of a quadruplex of molecular weight 6300 Da. If there were long-lived spermine-binding sites on TGT, the apparent correlation time would be much longer then 0.3 ns and would be expected to generate negative NOEs. The nulled NOEs are consistent with a mobile spermine that is essentially delocalised on the surface of TGT with no long-lived TGT binding site. All the spermine NOE peaks in the spectra of the other complexes are negative with the weakest being spermine:Myc2345 and the strongest, spermine:Myc12345 (Fig. 2B–E). The negative NOEs are evidence for an apparent correlation time for spermine associated with the single-stranded folded quadruplexes that is longer than 0.3 ns. This indicates the independent rotational and translational motions of spermine are attenuated, which is consistent with a longer residence time at one or more specific quadruplex binding sites where spermine mobility is restricted. The intramolecular spermine NOEs have uniformly greater intensity in the spermine:Myc12345 complex compared to the other quadruplexes indicating spermine has the longest residence time at the binding site(s) on Myc12345 (Fig. 2E and Table 2). Furthermore, the α2″-β NOE intensity is comparable to the α2″-γ NOE intensity (Fig. 2E) indicating that spermine bound to Myc12345 favours a *gauche* conformation about the C6–C7 and C6′–C7′ bonds because, in the all-*trans* conformation, the α2″-β$^1$H distances are too long to generate a substantial NOE [18]. The normalised NOE peak intensities are summarised in Table 2.

**Table 2**
Intramolecular $^1$H NOEs from the 1D-SCP(a2″)-NOESY spectra in Fig. 2A–E and the β/γ peak intensity ratio from the 1D(α1,α2′)-zTOCSY spectra in Fig. 2F–J.

| Oligonucleotide | Normalised NOE intensity[a] | | | TOCSY ratio |
|---|---|---|---|---|
| | α1 + α2′ | γ | β | β/γ |
| Myc12345 | 41.7 | 6.3 | 6.7 | 0.15 |
| Myc1234 | 20.0 | 3.5 | 2.8 | 0.27 |
| Myc2345 | 12.9 | 1.3 | 0.8 | 0.29 |
| VEGFT | 11.8 | 1.9 | 0.8 | 0.28 |
| TBA | 14.7 | 3.2 | 2.0 | 0.11 |
| TGT | <1 | <0.2 | <0.2 | 0.86 |

[a] Arbitrary units normalised relative to the source peak area (set to a value of 100). All NOEs were recorded at a NOESY mixing time of 200 ms.

The 1D(α1,α2′)-zTOCSY spectra (Fig. 2F–J) complement the NOE data. The α1,α2′ resonance at ~3.15 ppm is selectively excited followed by a 33 ms DIPSI-2 mixing period. Magnetisation is transferred from α2′ to γ and from α1 to β. The intensities of the β and γ peaks report on the relative transfer efficiency of the α2′−γ and the α1-β TOCSY pathways (Fig. 2) and the respective conformations about the C2–C3 and C6–C7 bonds. A less efficient transfer of magnetisation is indicative of a greater population of *gauche* conformers [18]. More efficient transfer of magnetisation indicates the *trans* conformation is predominant because of the large $^3J_{HH}$. The near equal intensity of the β and γ TOCSY peaks in Fig. 2F is in accord with a mobile and predominantly all-*trans* spermine that is trapped within the negative electrostatic field of TGT. In all the other complexes, the TOCSY transfer efficiency is much greater for the α2′−γ pathway compared to the α1−β pathway as shown by the relative peak intensities at the β and γ peaks (Fig. 2G–J) and numerically by the β/γ ratio of the integrated peak intensities in Table 2. The greater population of *gauche* conformers at the C6–C7 and C6′–C7′ bonds creates a curve or a bend in the spermine molecule, which brings the central nitrogens closer together to better match the distance between the adjacent phosphates and the curvature of the quadruplex backbone [18].

Previously, we showed by NMR and modelling that spermine is curved to match the shape of the narrow grooves of the thrombin-binding aptamer and is in close proximity to the loops that cap the narrow grooves [18]. Collectively, the NOE and TOCSY peak intensities in Fig. 2 and Table 2 indicate that spermine is also curved (or bent) when bound at specific sites on parallel quadruplexes with chain-reversal loops and the averaged degree of immobility is similar or greater when compared to spermine associated with TBA. The population-averaged immobility of spermine is enhanced in the presence of the fifth G-tract, but there does not appear to be an accompanying change in the G-quadruplex structure, which suggests a direct involvement of the fifth G-tract in the immobilisation of spermine. There is abundant evidence that nucleotides flanking the G-quadruplex, especially purines, are not mobile but rather protect the external G-quartets by stacking over them either as base-pairs or base-triples [11,25,31]. The presence of guanine in these flanking regions may be necessary if optimum stacking and

inter-base interactions require a *syn* guanine. Where the flanking nucleotides do stack over the external G-quartet, the backbone folds back forming a pocket where the spermine may partly reside. There are no detailed models of Pu27 or My12345 because, *in vitro*, these sequences form multiple quadruplex structures. We chose to model the curved spermine on the solution structure of a structural analogue of the Myc2345 G-quadruplex (PDB ID: 1XAV) [25]. We have manually superimposed spermine over the region of greatest negative charge density on the groove formed by the 2-nt chain-reversal loop and G-tract II. Four phosphates belonging to G13, T14, A15 and G16 are in close proximity and are oriented inward toward the centre line of the groove (Fig. 3). The binding position was optimised using the program, DOCK v6.5 [27]. The spermine is located over the 2-nt chain-reversal loop traversing the three G-quartets into a region where the 5′-terminal TGA sequence folds back under the external G-quartet (Figs. 3 and S3). The curved spermine follows the natural curvature of the quadruplex backbone (Fig. S3B) optimising contacts between the spermine amino groups and the quadruplex phosphates. N1 of spermine is proximal to the T14 phosphate at the apex of the chain reversal loop, N5 is located between the phosphates of G13 and A15, N5′ is near the A15 and G16 phosphates and N1′ is near the G16 phosphate. We speculate that the 5′-terminal TGGGGA sequence of Myc12345 folds back and contributes a negatively charged binding pocket that aids in immobilising spermine at the N1′ terminus and slowing the exchange with delocalised spermine. Fig. S4 illustrates a stick model of the curved spermine inserting laterally over a groove on the 1XAV electrostatic potential energy surface formed by the 2-nt chain-reversal loop and the second and third strands of the quadruplex. We also considered the possibility of a spermine binding site in the long loop of the 1:6:1 quadruplex isomer, which is a minor and less stable quadruplex component of the native Pu27 sequence. But we did not see any substantial change in the CD spectrum of Myc12345 on titration with spermine, which might be expected if spermine preferentially stabilised the 1:6:1 quadruplex isomer. Moreover, there was no observable change in the SCP-NOESY spectra at 0.5:1 and 1:1 spermine:Myc12345 (Fig. S5) suggesting that there is one preferred spermine binding site, which is located on the major 1:2:1 quadruplex species. Further work is necessary to fully characterise the association of spermine with Myc12345 and close analogues.

Polyamines influence the transcription of many growth-related genes either by altering the DNA structure or the equilibrium of duplex versus alternative structures, by modulating the recognition of proteins and small molecules or through regulating chromatin remodelling. There has been a recent focus on spermine-induced stabilisation of G-quadruplex structures but our experience is that, *in vitro*, most are already very stable at reasonable cation concentrations and it is the flexible spermine that adjusts its conformation to complement the optimum binding site. However, *in vivo*, under the influence of negative supercoiling, spermine may direct the folding of the flanking regions, which undoubtedly have an important structural and functional role. The dynamic charge distribution at the promoters, mediated by the preferred spermine residence sites at the nuclease hypersensitive elements, may also influence and possibly guide protein binding and chromatin remodelling. This work shows that the quadruplex structure is only part of the template necessary for the highest affinity spermine-binding site at the c-*Myc* NHE $III_1$. Further work is necessary to unravel the complex interaction of the quadruplex topology, and the differential polyamine and protein binding to these topologies that permits the quadruplex formation to alternatively act as a repressor or an enhancer depending on the local cellular environment.

In summary, we have shown that the nucleotides flanking the G-quadruplex in the c-*Myc* NHE $III_1$ have a role in restricting the mobility of spermine. This work emphasises that flanking nucleotides should not be ignored in structural and mechanistic studies of G-quadruplexes. Detailed knowledge of the structure of the flanking nucleotides may form the basis for the design of selective quadruplex-binding drugs.

## Acknowledgements

The work was supported by The Research School of Chemistry at The Australian National University.

## Appendix A. Supplementary data

Supplementary data associated with this article can be found, in the online version, at http://dx.doi.org/10.1016/j.febslet.2014.04.003.

## References

[1] Wang, J.Y., McCormack, S.A., Viar, M.J., Wang, H., Tzen, C.Y., Scott, R.E. and Johnson, L.R. (1993) Decreased expression of the proto-oncogenes *c-fos*, *c-myc* and *c-jun* following polyamine depletion in IEC-6 cells. Am. J. Physiol. 265, G331–G338.
[2] Thomas, T. and Thomas, T.J. (2001) Polyamines in cell growth and cell death: molecular mechanisms and therapeutic applications. Cell. Mol. Life Sci. 58, 244–258.
[3] Gerner, E.W. and Meyskens Jr., F.L. (2004) Polyamines and cancer: old molecules new understanding. Nat. Rev. 4, 781–792.
[4] Liu, B., Liang, X., Scott, G.K., Chang, C.-H., Baldwin, M.A., Thomas, T. and Benz, C.C. (1998) Polyamine inhibition of estrogen receptor (ER) DNA-binding and ligand binding functions. Breast Cancer Res. Treat. 48, 243–257.
[5] Berberich, S.J. and Postel, E.H. (1995) PuF/NM23-H2/NDPK-B transactivates a human c-myc promoter-CAT gene via a functional nuclease hypersensitive element. Oncogene 10, 2343–2347.
[6] Siddiqui-Jain, A., Grand, C.L., Bearss, D.J. and Hurley, L.H. (2002) Direct evidence for a G-quadruplex in a promoter region and its targeting with a small molecule to repress c-*MYC* transcription. Proc. Natl. Acad. Sci. USA 99, 11593–11598.
[7] Kumar, N., Basundra, R. and Maiti, S. (2009) Elevated polyamines induce *c-MYC* overexpression by perturbing quadruplex-WC duplex equilibrium. Nucleic Acids Res. 37, 3321–3331.
[8] Hurley, L.H., von Hoff, D.D., Siddiqui-Jain, A. and Yang, D. (2006) Drug targeting of the c-MYC promoter to repress gene expression via a G-quadruplex silencer element. Semin. Oncol. 33, 498–512.
[9] Phan, A.T., Modi, Y.S. and Patel, D.J. (2004) Propeller-type parallel-stranded G-quadruplexes in the human c-myc promoter. J. Am. Chem. Soc. 126, 8710–8716.
[10] Sun, D. and Hurley, L.H. (2009) The importance of negative superhelicity in inducing the formation of G-quadruplex and i-motif structures in the c-Myc promoter: implications for drug targeting and control of gene expression. J. Med. Chem. 52, 2863–2874.
[11] Mathad, R.I., Hatzakis, E., Dai, J. and Yang, D. (2011) C-MYC promoter G-quadruplex formed at the 5′-end of NHE $III_1$ element: insights into biological relevance and parallel-stranded G-quadruplex stability. Nucleic Acids Res. 39, 9023–9033.
[12] Van Dam, L. and Nordenskiöld, L. (1999) Interactions of polyamines with the DNA octamers $d(m^5CG)_4$ and d(GGAATTCC): a $^1$H-NMR investigation. Biopolymers 49, 41–53.
[13] Wemmer, D.E., Srivenugopal, K.S., Reid, B.R. and Morris, D.R. (1985) Nuclear magnetic resonance studies of polyamine binding to a defined DNA sequence. J. Mol. Biol. 185, 457–459.
[14] Egli, M. (2002) DNA–cation interactions: Quo vadis? Chem. Biol. 9, 277–286.
[15] Banville, D.L., Feuerstein, B.G. and Shafer, R.H. (1991) $^1$H and $^{31}$P nuclear magnetic resonance studies of spermine binding to the Z-DNA form of $d(m^5CGm^5CGm^5CG)_2$: evidence for decreased spermine mobility. J. Mol. Biol. 219, 585–590.
[16] Keniry, M.A. (2003) A comparison of the association of spermine with duplex and quadruplex DNA by NMR. FEBS Lett. 542, 53–158.
[17] Keniry, M.A. and Owen, E.A. (2007) An investigation of the dynamics of spermine bound to duplex and quadruplex DNA by $^{13}$C NMR Spectroscopy. Eur. Biophys. J. 36, 637–646.
[18] Keniry, M.A. and Owen, E.A. (2013) Insight into the molecular recognition of spermine by DNA quadruplexes from an NMR study of the association of spermine with the thrombin-binding aptamer. J. Mol. Recog. 26, 308–317.
[19] Kumar, N. and Maiti, S. (2008) A thermodynamic overview of naturally occurring intramolecular DNA quadruplexes. Nucleic Acids Res. 36, 5610–5622.
[20] Sun, D.Y., Guo, K.X., Rusche, J.J. and Hurley, L.H. (2005) Facilitation of a structural transition in the polypurine/polypyrimidine tract within the proximal promoter region of the human VEGF gene by the presence of

potassium and G-quadruplex-interactive agents. Nucleic Acids Res. 33, 6070–6080.
[21] Bock, L.C., Griffin, L.C., Latham, J.A., Vermaas, E.H. and Toole, J.J. (1992) Selection of single-stranded-DNA molecules that bind and inhibit human thrombin. Nature 355, 564–566.
[22] Aboul-ela, F., Murchie, A.I. and Lilley, D.M. (1992) NMR study of parallel-stranded tetraplex formation by the hexadeoxynucleotide d($TG_4T$). Nature 360, 280–282.
[23] Sklenár, V. and Bax, A. (1987) Spin-echo water suppression for the generation of pure-phase two-dimensional NMR spectra. J. Magn. Reson. 74, 469–479.
[24] Stott, K., Stonehouse, J., Hwang, T.-L., Keeler, J. and Shaka, A.J. (1995) Excitation sculpting in high-resolution nuclear magnetic resonance spectroscopy: application to selective NOE experiments. J. Am. Chem. Soc. 117, 4199–4200.
[25] Ambrus, A., Chen, D., Dai, J., Jones, R.A. and Yang, D.Z. (2005) Solution structure of the biologically relevant G-quadruplex element in the human c-myc promoter. Implications for G-quadruplex stabilization. Biochemistry 44, 2048–2058.
[26] Pettersen, E.F., Goddard, T.D., Huang, C.C., Couch, G.S., Greenblatt, D.M., Meng, E.C. and Ferrin, T.E. (2004) UCSF Chimera-a visualization system for exploratory research and analysis. J. Comput. Chem. 25, 1605–1612.
[27] Lang, P.T., Brozell, S.R., Mukherjee, S., Pettersen, E.T., Meng, E.C., Thomas, V., Rizzo, R.C., Case, D.A., James, T.L. and Kuntz, I.D. (2009) DOCK 6: combining techniques to model RNA-small molecule complexes. RNA 25, 1219–1230.
[28] Baker, N.A., Sept, D., Joseph, S., Holst, M.J. and McCammon, J.A. (2001) Electrostatics of nanosystems: application to microtubules and the ribosome. Proc. Natl. Acad. Sci. USA 98, 10037–10041.
[29] Sanner, M.F., Olson, A.J. and Spehner, J.C. (1996) Reduced surface. an efficient way to compute molecular surfaces. Biopolymers 38, 305–320.
[30] London, R.E., Perlman, M.E. and Davis, D.G. (1992) Relaxation-matrix analysis of the transferred nuclear Overhauser effect for finite exchange rates. J. Magn. Reson. 97, 79–98.
[31] Phan, A.T., Kuryavyi, V., Gaw, H.Y. and Patel, D.J. (2005) Small-molecule interaction with a five-guanine-tract G-quadruplex structure from the human MYC promoter. Nat. Chem. Biol. 1, 167–173.